JOURNAL OF GEOPHYSICAL RESEARCH, VOL. , XXXX, DOI:10.1029/,

Ballooning Instability Induced Plasmoid Formation in Near-Earth Plasma Sheet

P. Zhu[1,2] and J. Raeder[3]

P. Zhu, 1500 Engineering Drive, Madison, WI 53706; J. Raeder, 39 College Road, Durham, NH 03824. (pzhu@wisc.edu; j.raeder@unh.edu)

[1]Department of Modern Physics, University of Science and Technology of China, Hefei, Anhui, China

[2]Department of Engineering Physics and Department of Physics, University of Wisconsin-Madison, Madison, Wisconsin, USA.

[3]Space Science Center and Physics Department, University of New Hampshire, Durham, New Hampshire, USA.

Abstract. The formation of plasmoids in the near-Earth magnetotail is believed to be a key element of the substorm onset process. The physical mechanism of plasmoid formation in the plasma sheet has remained a subject of considerable interests and investigations. Previous work has identified a new scenario in MHD simulations where the nonlinear evolution of a ballooning instability is able to induce the formation of plasmoids in a generalized Harris sheet with finite normal magnetic component [*Zhu and Raeder*, 2013]. In present work, we further examine this novel mechanism for plasmoid formation and explore its implications in the context of substorm onset trigger problem. For that purpose, we adopt the generalized Harris sheet as a model proxy to the near-Earth region of magnetotail during the substorm growth phase. In this region the magnetic component normal to the neutral sheet B_n is weak but nonzero. The magnetic field lines are closed and there are no X-lines. Simulation results indicate that in the higher Lundquist number regime $S \gtrsim 10^4$, the linear axial tail mode, which is also known as "two-dimensional resistive tearing mode", is stabilized by the finite B_n, hence cannot give rise to the formation of X-lines or plasmoids by itself. On the other hand, the linear ballooning mode is unstable in the same region and regime, and in its nonlinear stage, the tailward stretching of the plasma sheet in the closed field line region due to the growing ballooning finger structures tends to accelerate the thinning of the near-Earth current sheet. This eventually leads to the formation of a series of plasmoid structures in the near-Earth and middle magnetotail regions of plasma sheet. This new scenario of plasmoid for-

mation suggests a critical role of ballooning instability in the near-Earth plasma sheet in triggering the onset of a substorm expansion.

1. Introduction

Plasmoids are often found in natural and laboratory plasmas in association with various eruptive processes, such as those observed in solar corona, magnetosphere, and magnetic fusion experiments. In general, the concept of plasmoid may well be an approximate characterization for a range of bounded 2D regions of projections of the more complicated three-dimensional (3D) magnetic flux structures. Whereas the precise definition of plasmoid may have yet to be found, the term plasmoid often refers to a finite two-dimensional (2D) region of closed magnetic flux bounded by a separatrix, usually with a single X-point, particularly in the context of space plasmas [*Otto et al.*, 1990; *Biskamp*, 1993]. For future reference, we call them "type-1 plasmoids" in the rest of this paper. Under certain conditions, isolated secondary magnetic islands can spontaneously form in the downstream region of a Sweet-Parker current sheet, which are also generally referred to as plasmoids in literature (e.g. [*Biskamp*, 1993; *Loureiro et al.*, 2007; *Bhattacharjee et al.*, 2009]). We refer to these secondary islands as the"type-2 plasmoids" here. Unlike the type-1 plasmoid, a typical magnetic island is usually bounded by separatrix with two X-points. Besides the difference in geometry, the type-1 plasmoids are mostly generated from current sheets with finite normal magnetic component where no X-point (X-line) or reconnection process pre-exists. In contrast, the type-2 plasmoids, or secondary islands, originate from the neutral line region of the Sweet-Parker type current sheet in presence of the primary reconnection process. Such a distinction between the two types of plasmoids may be necessary to understand the physics associated with each type of plasmoids, which can be related but different. In this paper, we limit our discussions to the original type-1 plasmoids commonly found in the solar and magnetospheric magnetic configurations.

The formation of plasmoids in the near-Earth magnetotail has long been believed a key element in various scenarios of the substorm onset process. One such early substorm scenario was based on the idea originally suggested by *Hones Jr.* [1977] that the neutral line and the resulting plasmoid can spontaneously form in the near-Earth region of magnetotail near the end of the substorm growth phase, presumably through the onset of a tearing mode instability. Since 1960s, the tearing instability and the plasmoid formation in the plasma sheet have remained a subject of considerable interests and investigations.

The concept of tearing mode was originally conceived for the Harris type, one-dimensional (1D) current sheets, where anti-parallel magnetic field lines are separated by an pre-existing neutral line [*Furth et al.*, 1963]. The intuitive picture of the process involves a change of topology through a “tearing” of magnetic field lines and their subsequent reconnection. The concept and analysis of the tearing mode in the Harris sheet (hereafter referred to as “1D tearing mode”) has since been applied to the near-Earth magnetotail configuration, despite the fact that the current sheet there has no pre-existing X-line due to the presence of finite magnetic component normal to the current sheet neutral line (e.g. [*Schindler*, 1974; *Galeev and Zelenyi*, 1976; *Birn et al.*, 1975; *Birn*, 1980; *Janicke*, 1980; *Hesse and Birn*, 1994; *Harrold et al.*, 1995; *Sundaram and Fairfield*, 1997; *Sitnov et al.*, 2002]). The current sheet in near-Earth magnetotail is commonly modeled as a two-dimensional (2D), generalized Harris sheet, where the finite magnetic component normal is weak but nonzero. In MHD models, such a 2D current sheet can become unstable to the resistive instability that are historically referred to as “2D resistive tearing mode" [*Schindler*, 1974; *Galeev and Zelenyi*, 1976; *Birn et al.*, 1975; *Birn*, 1980; *Janicke*, 1980; *Hesse and Birn*, 1994]. However, the finite normal magnetic component (denoted as B_n) has been found to have a strong stabilization effects on the 2D resistive tearing mode [*Harrold et al.*, 1995; *Sundaram and Fairfield*, 1997]. For the nearly collisionless regime of magnetotail plasma, the 2D resistive tearing mode is essentially stable in the framework of MHD model.

Collisionless kinetic models have also been employed to address the question whether the 2D current sheet in near-Earth magnetotail can spontaneously form X-line through the tearing-like perturbations. It was first revealed by *Lembége and Pellat* [1982] that the 2D ion tearing mode is stable in current sheets with finite B_z due to the magnetization of electrons. Similar results were obtained later in theory analyses [*Pellat et al.*, 1991; *Brittnacher et al.*, 1994; *Quest et al.*, 1996] and particle-in-cell (PIC) simulations [*Pritchett*, 1994; *Pritchett and Büchner*, 1995]. Lately, 2D PIC simulations have found slowly growing modes on closed field lines for a certain type of multi-scale generalized Harris sheets [*Sitnov and Swisdak*, 2011]. It remains an unresolved question how plasmoids would spontaneously form from small fluctuations at a significantly faster sub-Alfvénic time scale on closed field lines in the collisionless near-Earth magnetotail.

Previous analyses and simulations on the resistive instability of the magnetotail configuration were mostly conducted in the low Lundquist number regimes where the linear 2D resistive tearing mode is unstable [*Birn and Hones, Jr.*, 1981; *Lee et al.*, 1985; *Hautz and Scholer*, 1987; *Ugai*, 1989; *Otto et al.*, 1990; *Kageyama et al.*, 1990; *Biskamp*, 1993]. Recently our numerical simulation suggests that the ballooning instability of the near-Earth magnetotail can induce the formation of plasmoids in the low collisionality regimes where the linear 2D resistive tearing mode itself is stable [*Zhu and Raeder*, 2013]. Our recent three dimensional (3D) MHD simulations of plasmoid formation process in the current sheet with finite B_n and weak resistivity have shown significant difference from 2D simulations due to the 3D effects. In particular, the inclusion of the spatial variation in the equilibrium current direction (which is y direction in the Cartesian coordinates defined later) allows the presence of ballooning instability, which has demonstrated its critical roles in the plasmoid formation process in the higher Lundquist number regimes where the linear 2D resistive modes of the current sheet are stable. In present work, we further examine the critical roles of ballooning instability in the novel mechanism for plasmoid formation and explore its implications in the context of substorm onset trigger problem. For that purpose, we adopt the generalized Harris sheet as a model proxy to the near-Earth region of magnetotail during the substorm growth phase, and conduct a comprehensive range of simulations in various physical scenarios and numerical settings. These simulation results further confirm the viability of the new mechanism for plasmoid formation in the more realistic collisionality and configuration regimes of the near-Earth magnetotail. We report and discuss the details of these findings in next sections.

2. Generalized Harris Sheet Model of near-Earth Magnetotail

The near-Earth magnetotail configuration ($\sim 6-30 R_{\rm E}$) during the slow growth phase of substorms can be modeled as a generalized Harris sheet in GSM coordinates (x, y, z) where $\mathbf{B}_0(x,z) = \mathbf{e}_y \times \nabla\Psi(x,z)$, $\Psi(x,z) = -\lambda \ln\{\cosh[F(x)z/\lambda]/F(x)\}$, and $\ln F(x) = -\int B_{0z}(x,0)dx/\lambda$. Here λ is the current sheet width, $\mathbf{e}_y$ the unit vector in y direction, and all other symbols are conventional. Thus a generalized Harris sheet is to a large extent determined by the profile of $B_n = B_{0z}(x)$, where B_n is the magnetic component normal to neutral sheet or equatorial plane at $z = 0$. Observations have indicated the presence of a minimum B_z region in the near-Earth magnetotail during the substorm growth phase (e.g. [*Sergeev et al.*, 1994; *Saito et al.*, 2010]), which could be a consequence of the adiabatic magnetotail convection [*Erickson and Wolf*, 1980], or the azimuthal channel of magnetic flux transport induced by the dayside magnetic reconnection [*Otto and Hsieh*, 2012]. Global MHD simulations have also found the minimum B_z region in near-tail plasma sheet prior to substorm onset [*Raeder et al.*, 2008; *Zhu et al.*, 2009]. For those reasons, we adopt a $B_{0z}(x,0)$ profile with a minimum region along the x axis (Fig. 1) for the generalized Harris sheet configuration in our work. The same type of $B_{0z}(x,0)$ profiles were also used to model the near-Earth magnetotail in many previous studies [*Schindler*, 1972; *Pritchett and Büchner*, 1995; *Zhu et al.*, 2013; *Zhu and Raeder*, 2013]. Here $B_{0z}(x,0)$ is a piece-wise linear function of x which assumes a simple analytic form

$$B_{0z}(x,0) = \begin{cases} \epsilon_1 \frac{x-x_1}{x_1-x_0} + B_{\min} & x_0 < x < x_1 \\ B_{\min} & x_1 < x < x_2 \\ \epsilon_2 \frac{x-x_2}{x_3-x_2} + B_{\min} & x_2 < x < x_3 \\ \epsilon_2 + B_{\min} & x > x_3 \end{cases}, \tag{1}$$

where x_i $(i = 0,1,2,3)$, ϵ_i $(i = 1,2)$, and $B_{\min}$ are parameters that define the profile of $B_{0z}(x,0)$. The discontinuity in the derivative $\partial B_{0z}(x,0)/\partial x$ however does not affect the validity of our results. In Sec. 7, we demonstrate this by presenting the simulation results based on a similar but more realistic generalized Harris sheet configuration where $B_{0z}(x,0)$ is continuous in x at any differential order.

3. Resistive MHD Model

To further investigate the stability of the generalized Harris sheet configuration in higher Lundquist number regime, a full set of resistive MHD equations are solved in 3D domain as an initial-boundary value problem

$$\frac{\partial \rho}{\partial t} + \nabla \cdot (\rho \mathbf{u}) = 0 \tag{2}$$

$$\rho \left(\frac{\partial \mathbf{u}}{\partial t} + \mathbf{u} \cdot \nabla \mathbf{u} \right) = \mathbf{J} \times \mathbf{B} - \nabla p + \mu \nabla \cdot (\rho \mathbf{w}) \tag{3}$$

$$\frac{\partial p}{\partial t} + \mathbf{u} \cdot \nabla p = -\gamma p \nabla \cdot \mathbf{u} \tag{4}$$

$$\frac{\partial \mathbf{B}}{\partial t} = -\nabla \times \mathbf{E} \tag{5}$$

$$\mathbf{E} = -\mathbf{u} \times \mathbf{B} + \eta \mathbf{J} \tag{6}$$

$$\mu_0 \mathbf{J} = \nabla \times \mathbf{B} \tag{7}$$

where ρ is the mass density, $\mathbf{u}$ the plasma flow velocity, p the pressure, $\mathbf{E}$ the electric field, $\mathbf{B}$ the magnetic field, $\mathbf{J}$ the current density, the adiabatic index or specific ratio $\gamma = 5/3$, and $\mathbf{w} = \nabla \mathbf{u} + (\nabla \mathbf{u})^{\mathrm{T}} - \frac{2}{3}\mathbf{I}\nabla \cdot \mathbf{u}$ is the rate-of-strain tensor. In a weakly collisional or collisionless plasma the effective resistivity η and viscosity μ are small in absence of anomalous sources. The above set of equations have been implemented in both the linearized and the fully nonlinear version in the NIMROD code [*Sovinec et al.*, 2004] used in our computation. A solid, no-slip wall boundary condition has been imposed on the sides of the computation domain in both x and z directions, so that any potential influence from an external driver or inward flow may be excluded. The boundary condition in the y direction is periodic. The spatial and temporal variables are normalized with the equilibrium scale length (e.g. Earth radius) and the Alfvénic time τ_{A}, respectively.

4. Plasmoid Formation due to 2D Tearing or Axial Tail Instability Alone

The generalized Harris sheet model of near-Earth magnetotail configuration considered in the previous section has been known to be unstable to the linear 2D resistive tearing mode in the low Lundquist number regime for sufficiently small B_z(e.g. [*Schindler*, 1974;

Galeev and Zelenyi, 1976; *Birn et al.*, 1975; *Birn*, 1980; *Janicke*, 1980; *Hesse and Birn*, 1994; *Harrold et al.*, 1995; *Sundaram and Fairfield*, 1997; *Sitnov et al.*, 2002]). Such a linear 2D resistive instability has been interpreted as the "axial tail instability" in the context of substorm physics in an effort to distinguish the nature of the instability from that of magnetic reconnection [*Raeder et al.*, 2010; *Zhu et al.*, 2013], which is often attributed to the underlying process of conventional tearing modes. During the nonlinear stage, the axial tail instability can eventually reduce the equilibrium B_z component to zero around the minimum B_z region along x direction, thus leads to the formation of an X-line and a plasmoid. One such example is shown in Fig. 2, where the plasmoid structure results from the nonlinear evolution of an axial tail instability developed from the near-Earth magnetotail configuration represented in Fig. 1 for the Lundquist number $S = 10^3$. However, such a process is rather slow; it takes about $8000\tau_{\mathrm{A}}$ for the plasmoid to fully develop. The nonlinear evolution of the axial tail instability is not faster than its corresponding linear phase.

5. Linear Finite-k_y Ballooning Instability

Linear calculations indicate that the current sheet configuration shown in Fig. 1 is unstable to modes with finite-k_y wavenumbers. The inclusion of spatial variation in the y direction significantly enhances the linear growth, particularly in the higher S regime when the zero-k_y 2D resistive tearing or axial tail mode is stable (Fig. 3). The enhanced linear growth of the finite-k_y instability remains effective and becomes more relevant in the more realistic collisionality regime ($S \gtrsim 10^6$), thus making the instability a viable mechanism for explaining the faster sub-Alfvénic time scale of the near-Earth magnetotail disruption in situations where the sources for large anomalous resistivity are not available. As k_y

increases, the growth rates become less sensitive to the resistivity, indicating a transition from resistive to ideal MHD ballooning mode regime.

Note that the magnetic Prandtl number $P_m = \mu/\eta = 1$ is fixed for all the cases, thus as the resistivity η decreases (i.e. S increases) the viscosity μ also decreases. For the low-k_y resistive modes considered here, the effect of resistivity is destabilizing whereas that of viscosity is stabilizing. Fig. 3 shows two regimes in Lundquist number S for the low k_y modes (i.e. $2\pi/k_y > 10$). In the first regime ($S \lesssim 10^5$), the growth rates decrease with S, indicating that the stabilizing effect due to the decreasing resistivity (or increasing S) is dominant. In the second regime ($S \gtrsim 10^5$), the growth rates appear to increase with S. This is because in this regime the destabilizing effect from decreasing viscosity μ starts to overcome the stabilizing effect due to decreasing resistivity η (or increasing S).

For a finite-k_y ballooning instability in the model configuration of near-Earth magnetotail, the linear mode structure is characterized by a mixture of characteristics from both axial tail and ballooning instabilities in the $x - z$ plane (Fig. 4). On the one hand, the mode distribution tends to be spatially aligned along the magnetic field lines, as can be observed from the contour plots of the perturbed pressure, and the x components of the perturbed flow and magnetic field, which is one of the signatures of linear ballooning mode structure. On the other hand, the global mode structure in $x - z$ plane of the $k_y = 0.2\pi$ ballooning instability also resembles that of the axial tail or 2D resistive tearing mode in such a magnetotail configuration in terms of symmetries in both x and z directions, as can be seen in comparison with Fig. 2 of [*Zhu et al.*, 2013]. The merging of the mode structures in $x - z$ plane indicates that there is a coupling between the driving mechanisms for ballooning instability and axial tail mode. Such a coupling may persist in the nonlinear stage and lead to the rapid onset of reconnection and formation of plasmoids.

6. Plasmoid Formation Induced by Nonlinear Finite-k_y Ballooning Instability

We now consider the nonlinear plasmoid formation process in the same current sheet configuration in a higher Lundquist number regime $S = 10^4$ where the 2D resistive tearing mode is linearly stable and a plasmoid cannot spontaneously form internally from a purely 2D linear process ($k_y = 0$). The inclusion of the 3D effects leads to an entirely new scenario where the plasmoid formation can be nonlinearly driven by a finite-k_y ballooning instability. We report in details two simulation cases to demonstrate this scenario.

6.1. Initial perturbation with nonzero single k_y component

We previously reported results demonstrating such a scenario from a representative numerical case with a minimal spatial resolution [*Zhu et al.*, 2013]. Here we show that the scenario persists when the spatial resolution in the y direction is doubled, thus providing evidence for the numerical convergence of our previous results. The simulation is initialized with small magnetic perturbation whose magnitude is about one tenth of the minimum B_n. The initial perturbation is monochromatic in the y direction with a wavelength satisfying $k_y L_y/2\pi = 10$, where $L_y = 100$ is the domain size in y. A finite element mesh of 64×64 with a polynomial degree of 5 in each direction is used for the $x - z$ domain of $x \in [6, 26], z \in [-3, 3]$. In the y direction, 64 Fourier collocation points are used to resolve Fourier components in the range of $0 \leq k_y L_y/2\pi \leq 20$. The perturbation quickly settles into a linearly growing ballooning instability first, and subsequently drives the growth of the $k_y = 0$ component and the secondary harmonic component ($k_y L_y/2\pi = 20$) through nonlinear coupling (Fig. 5). As described in details next, the simulation results here with higher spatial resolution confirms the previous finding reported by *Zhu et al.* [2013] that nonlinear ballooning instability can drive the spontaneous formation of plasmoid chains in the $x - z$ plane.

In particular, our simulations have reproduced the major stages of plasmoid formation following the nonlinear growth of ballooning instability (Fig. 6). The nonlinear ballooning growth is characterized by the growing ballooning finger-like structures in the $z = 0$ plane extending in the x direction, as represented by the plot at $t = 160$ (the upper left panel in Fig. 6). The magnetic field lines are mostly frozen-in to the plasma and they move along with the extending fingers, which results in a stretching and thinning of the current sheet. The reduction of the normal component B_n in the $z = 0$ plane appears to be the most in extent near the moving fronts of the extending fingers, as evidenced by the formation of a plasmoid in one of those locations around $x = 14$ at $t = 170$ (the upper right panel in Fig. 6). In addition to the formation of plasmoid in close association with the extruding fronts of nonlinear ballooning fingers, other plasmoids have also started to form later in the wake of those ballooning finger fronts. During this stage, a second plasmoid is observed to appear around $t = 200$ on those magnetic field lines crossing the $z = 0$ plane in the region around $x \simeq 9$. The first plasmoid previously located near $x = 14$ has now moved to the location $x \gtrsim 15$ (the lower left panel in Fig. 6). In the next stage, a third plasmoid appears by the time $t = 210$ near $x = 12.5$ between the locations of the two plasmoids previously formed which continue to exist. The location of the first plasmoid has now moved back to $x \lesssim 14$, whereas the second plasmoid remains to be around $x \simeq 9$ (the lower right panel in Fig. 6).

Unlike in 2D simulations, the above 3D plasmoid formation process is different for different locations along y direction. For example, for a different set of field lines crossing the x axis at $y = -0.95, z = 0$, there is no plasmoid structure in locations $x \gtrsim 15$ at $t = 200$, but a different plasmoid structure forms around $x = 12.75$ (Fig. 7, left panel). Similarly at the later time $t = 210$, the simultaneous appearance of three plasmoid structures on the set of field lines crossing the x axis at $y = -0.9, z = 0$ is absent on the set of field lines crossing the x axis at $y = -0.95, z = 0$, where the pattern of plasmoid distribution is different (Fig. 7, right panel). In particular, the plasmoids at $x = 9$ and $x = 12.5$ disappeared, whereas the plasmoid at $x \lesssim 14$ is now replaced by a nearby plasmoid structure at $x = 13.5$ with a different geometry shape. Similar to that reported in [*Zhu et al.*, 2013], the variation of the plasmoid presence in the y direction strongly indicates that the plasmoid formation process reported here is an intrinsically 3D process.

6.2. Initial perturbation with nonzero multiple k_y components

In the above case, the initial perturbation is set up to be dominated by a single k_y Fourier component for the purpose of clearly illustrating the physical process. In the present case, we consider the same equilibrium of generalized current sheet in the Lundquist number regime of $S = 10^4$, but with a different initial perturbation where all k_y Fourier components are set up to have the same initial small amplitude, as a model representation of the more realistic situation. The simulation mesh and domain size in the $x - z$ plane remain the same as in the previous case. In the y direction, 32 Fourier collocation points are used to resolve Fourier components in the range of $0 \leq k_y L_y / 2\pi \leq 10$, where $L_y = 100$ continues to be the domain size in this dimension. All the 11 Fourier components of the initial magnetic perturbation in the y direction are initialized with the same amplitude of one-tenth the $B_{\min}$.

After an initial transient phase, the higher k_y components ($k_y L_y/2\pi \gtrsim 5$) of the initial perturbation start their linear growth phase (Fig. 8). During the early nonlinear phase ($t \gtrsim 70$), these exponentially growing k_y components drive the linearly stable, lower k_y components through nonlinear coupling. All k_y components begin to saturate by the time $t \gtrsim 150$, and the highest k_y component ($k_y L_y/2\pi = 10$) remains dominant. The plasmoid formation process can be visualized through a time sequence of two-dimensional projections of magnetic field streamlines into the $x - z$ plane ($y = 0$ or equivalently $y = 100$) (Fig. 9). The sequence starts at $t = 0$ and is shown at a time interval of $t = 20$ from $t = 90$ and $t = 250$. The major phases of plasmoid formation process are similar to the previous case. Before the appearance of plasmoid, the nonlinear growth of the ballooning instability induces tailward stretching of closed field lines in the equatorial plane and further thinning of current sheet ($t = 90$). Subsequently at $t = 110$ the first X-line originates around $x = 11$. The resulting plasmoid, along with the X-line, moves tailward and grows in size. A local dipolarization also occurs in association with the growing plasmoid by the time it reaches the middle tail region $x = 14$ around $t = 210$. Afterwards at $t = 230$, a second x-line and plasmoid start to develop in the near-Earth magnetotail region $x \lesssim 11$, in the wake of the first tailward moving plasmoid in the middle tail region.

The 2D projection of the plasmoid magnetic structure closely resembles the plasmoid structure in the 3D streamlines out of the same magnetic field. For example, the top panel of Fig. 10 shows the full 3D magnetic field streamlines crossing the x axis along

$y = -100$ in the $z = 0$ plane at $t = 250$, which capture the same two plasmoid structures as in the 2D projection at the same time shown in Fig. 9. These plasmoid structures are also intrinsically 3D as well, as they vary dramatically along y direction. For example, the plasmoid structures composed by the magnetic field streamlines crossing the ballooning finger locations (i.e. the local pressure maximum) along $y = -100$ in the $z = 0$ plane are totally absent on the magnetic field streamlines crossing the ballooning finger locations along $y = -50$ in the same $z = 0$ plane (Fig. 10, lower panel). Thus the entire global 3D magnetic structure of plasmoids can be quite different from the 2D projection of the magnetic structure on any particular plane.

Even within a 2D plane, the 2D projection of the 3D reconnection process associated with the plasmoid structure differs significantly from the anti-parallel reconnection process in the conventional Harris sheet configuration where $B_n = 0$ (Fig. 11). For the generalized Harris sheet considered here, the stagnation points in the tailward flow are in general not the same locations as the magnetic X-points or O-points of the plasmoid structures. Due the lack of the association between those locations, the flow pattern shown here no longer conforms clearly to the conventional in-flow or out-flow pattern in the Sweet-Parker like reconnection process. In fact, the flow patterns around and inside these plasmoids are rather complicated, which are composed of both layered and vortex structures. To certain extent, such a complex flow pattern may also be a reflection and consequence of the 3D nature of these reconnection processes.

7. Generalized Harris Sheet Model with Smooth B_n Profile

The new scenario for plasmoid formation reported in previous sections is not limited to the model current sheet defined by the $B_{0z}(x, 0)$ profile shown in Fig. 1. To demonstrate this, we have considered a similar generalized Harris sheet, but with a smooth hence more realistic $B_{0z}(x,0)$ profile that is continuous at any differential order (the upper row of Fig. 12). The $B_z(x,0)$ profile is defined as follows

$$B_{0z}(x,0) = B_m - B_1 \tanh\left(\frac{x-x_1}{d_1}\right) + B_2 \tanh\left(\frac{x-x_2}{d_2}\right), \tag{8}$$

where the parameters $B_m = 0.305$, $B_1 = 0.247$, $B_2 = 0.0522$, $x_1 = 8$, $x_2 = 12$, and $d_1 = d_2 = 1$ for the case shown in Fig. 12. The same process of plasmoid formation induced by the onset of nonlinear ballooning instability has been similarly reproduced for this new current sheet configuration. In the Lundquist number regime $S = 10^4$, this particular configuration is stable to the resistive 2D tearing or axial tail mode, and unstable to finite-k_y ballooning instability. Applying the same boundary conditions as in the case reported in Sec. 6.1 on a computational domain of $x \in [6:26], y \in [0:10], z \in [-3:3]$, we initialize the simulation with a perturbation that only the $k_y = 2\pi$ component has a nonzero amplitude. Following the linear and nonlinear growth of the ballooning instability, which is dominated by the $k_y = 2\pi$ component, simulation results indicate that a plasmoid structure appears at time $t = 140$ near the finger front of ballooning instability around $x = 14$ (the lower row of Fig. 12). This has further demonstrated the universal applicability of the plasmoid formation mechanism in the magnetotail configuration.

8. Summary and Discussion

In summary, we have reported the details of several simulation cases that have further demonstrated a new mechanism for the plasmoid formation and onset of reconnection in the near-Earth magnetotail region. Namely, our simulation results strongly indicate that the nonlinear ballooning instability can effectively enable the formation of plasmoids in the near-Earth magnetotail in the higher Lundquist number regime where the 2D resistive tearing or axial tail mode is stabilized by the finite B_n. Originally reported by *Zhu and Raeder* [2013] in a single proto-type setting and configuration, such a scenario has been shown to persist in the more general simulations conducted in this work with extended settings such as smooth $B_{z0}(x,0)$ profile, higher spatial resolutions, as well as non-monochromatic initial perturbations, respectively. Our work has demonstrated for the first time that as a macroscopic coherent process, the ideal MHD ballooning instability is capable of inducing the formation of plasmoids in the magnetotail configuration without relying on any microscopic, kinetic, or turbulent processes. In light of recent evidence found in ground and in-situ observations for the presence of ballooning instability in the pre-onset auroral and plasma sheet structures [*Saito et al.*, 2010, 2011; *Panov et al.*, 2012; *Motoba et al.*, 2012a, b], our findings on the ballooning instability induced plasmoid formation may indeed provide a solid and practical scheme for ballooning instability in the near-Earth magnetotail to play a critical role in triggering the substorm onset process.

Although our results are from resistive MHD simulations, they are really intended for the collisionless magnetotail regime where resistivity is so weak that the "2D resistive tearing" or axial tail mode ($k_y = 0$) alone is unable to grow. In the reported results, the dominant ballooning instability is actually ideal MHD in nature because its growth rate is insensitive to resistivity, and the weak resistivity here plays only a relatively minor role by allowing the secondary reconnection to occur. The current results are meant to be a first step to demonstrate that the ballooning process alone can act as an independent collisionless mechanism for plasmoid instability and formation in absence of other Hall or kinetic effects. Due to the ubiquitous presence of ballooning instability in a wide range of

MHD and kinetic regimes, the ballooning induced mechanism for plasmoid instability and formation is likely to prevail in two-fluid MHD and fully kinetic models for collisionless plasmas as well. It remains an open question whether kinetic effects that are not taken into account in our MHD simulations can prevent the formation of X-point and plasmoids. Recent 2D kinetic simulations have shown that kinetic effects can enable plasmoids to form in magnetotail configurations and regimes where the 2D resistive tearing mode itself would be stable [*Bessho and Bhattacharjee*, 2012; *Sitnov et al.*, 2013]. Previous 3D kinetic simulation found the onset of reconnection in the wake of an Earthward flow generated by the interchange instability [*Pritchett and Coroniti*, 2011]. However the causal relation between the interchange instability and the appearance of an X-point in their 3D kinetic simulation has not been rigorously established, because it is not demonstrated in their work whether the magnetotail current sheet considered would be indeed unstable to 2D tearing modes in absence of interchange instability. In order to further evaluate the kinetic effects, extending our current simulation work to the two-fluid and kinetic regimes, and conducting comparisons among MHD, two-fluid, and kinetic simulation results will be subject of future studies.

Acknowledgments. This research was supported by NSF grants AGS-0902360 and PHY-0821899. Work at UNH was also supported by NASA grant NAS5-02099 (THEMIS). P. Zhu is grateful for discussions with A. Bhattacharjee, J. Birn, N. Bessho, C. C. Hegna, Y.-M. Huang, C.-S. Ng, A. Otto, A. Runov, Z. J. Rong, M. Sitnov, C. R. Sovinec. The computational work used the NSF XSEDE resources provided by TACC under grant number TG-ATM070010, and the resources of NERSC, which is supported by DOE under Contract No. DE-AC02-05CH11231.

References

Bessho, N., and A. Bhattacharjee (2012), PIC simulation studies for instabilities in a current sheet with finite normal magnetic fields, in *American Geophysical Union Fall Meeting, San Francisco, CA, USA, December 3-7, 2012*, abstract SM52A-04.

Bhattacharjee, A., Y.-M. Huang, H. Yang, and B. Rogers (2009), Fast reconnection in high-lundquist-number plasmas due to the plasmoid instability, *Phys. Plasmas*, *16*, 112,102, doi:10.1063/1.3264103.

Birn, J. (1980), Computer studies of the dynamic evolution of the geomagnetic tail, *J. Geophys. Res.*, *85*, 1214–1222.

Birn, J., and E. W. Hones, Jr. (1981), Three-dimensional computer modeling of dynamic reconnection in the geomagnetic tail, *J. Geophys. Res.*, *86*(A8), 6802–6808, doi:10.1029/JA086iA08p06802.

Birn, J., R. Sommer, and K. Schindler (1975), Open and closed magnetospheric tail configurations and their stability, *Astrophys. Space Sci.*, *35*, 389.

Biskamp, D. (1993), *Nonlinear Magnetohydrodynamics*, Cambridge University Press, Cambridge, UK.

Brittnacher, M., K. B. Quest, and H. Karimabadi (1994), On the energy principle and ion tearing in the magnetotail, *Geophys. Res. Lett.*, *21 (15)*, 1591–1594, doi:10.1029/94GL01697.

Erickson, G. M., and R. A. Wolf (1980), Is steady convection possible in the Earth's magnetotail?, *Geophys. Res. Lett.*, *7*, 897.

Furth, H. P., J. Killeen, and M. N. Rosenbluth (1963), Finite resistivity instabilities of a sheet pinch, *Phys. Fluids*, *6*, 459, doi:10.1063/1.1706761.

Galeev, A. A., and L. M. Zelenyi (1976), Tearing instability in plasma configurations, *Sov. Phys. JETP*, *43*, 1113.

Harrold, B. G., A. Bhattacharjee, and X. G. Wang (1995), Tearing stability of the two-dimensional magnetotail, *Phys. Plasmas*, *2*, 3857–3864.

Hautz, R., and M. Scholer (1987), Numerical simulations on the structure of plasmoids in the deep tail, *Geophys. Res. Lett.*, *14*(9), 969–972, doi:10.1029/GL014i009p00969.

Hesse, M., and J. Birn (1994), MHD modeling of magnetotail instability for localized resistivity, *J. Geophys. Res.*, *99*, 8565–8576.

Hones Jr., E. W. (1977), Substorm processes in the magnetotail: Comments on 'On hot tenuous plasmas, fireballs, and boundary layers in the Earth's magnetotaili' by L. A. Frank, K. L. Ackerson, and R. P. Lepping, *J. Geophys. Res.*, *82*, 5633–5640, doi:10.1029/JA082i035p05633.

Janicke, L. (1980), Resistive tearing mode in weakly two-dimensional neutral sheets, *Phys. Fluids*, *23*, 1843–1849.

Kageyama, A., K. Watanabe, and T. Sato (1990), Global simulation of the magnetosphere with a long tail: The formation and ejection of plasmoids, *Tech. Rep. NIFS-049*, National Institute for Fusion Science.

Lee, L. C., Z. F. Fu, and S.-I. Akasofu (1985), A simulation study of forced reconnection processes and magnetospheric storms and substorms, *J. Geophys. Res.*, *90*(A11), 10,896–10,910, doi:10.1029/JA090iA11p10896.

Lembége, B., and R. Pellat (1982), Stability of a thick two-dimensional quasineutral sheet, *Phys. Fluids*, *25*, 1995.

Loureiro, N. F., A. A. Schekochihin, and S. C. Cowley (2007), Instability of current sheets and formation of plasmoid chains, *Phys. Plasmas*, *14*, 100,703, doi:10.1063/1.2783986.

Motoba, T., K. Hosokawa, A. Kadokura, and N. Sato (2012a), Magnetic conjugacy of northern and southern auroral beads, *Geophys. Res. Lett.*, *39*, L08,108, doi: 10.1029/2012GL051599.

Motoba, T., K. Hosokawa, Y. Ogawa, N. Sato, A. Kadokura, S. E. Milan, and M. Lester (2012b), Simultaneous ground-satellite observations of meso-scale auroral arc undulations, *J. Geophys. Res.*, *117*, A06,213, doi:10.1029/2011JA017291.

Otto, A., and M.-S. Hsieh (2012), Convection constraints and current sheet thinning during the substorm growth phase, in *American Geophysical Union Fall Meeting, San Francisco, CA, USA, December 3-7, 2012*, abstract SM11C-2314.

Otto, A., K. Schindler, and J. Birn (1990), Quantitative study of the nonlinear formation and acceleration of plasmoids in the earth's magnetotail, *J. Geophys. Res.*, *95*(A9), 15,023–15,037, doi:10.1029/JA095iA09p15023.

Panov, E. V., V. A. Sergeev, P. L. Pritchett, F. V. Coroniti, R. Nakamura, W. Baumjohann, V. Angelopoulos, H. U. Auster, and J. P. McFadden (2012), Observations of kinetic ballooning/interchange instability signatures in the magnetotail, *Geophys. Res. Lett.*, *39*, 8, doi:10.1029/2012GL051668.

Pellat, R., F. V. Coroniti, and P. L. Pritchett (1991), Does ion tearing exist?, *Geophys. Res. Lett.*, *18 (2)*, 143–146, doi:10.1029/91GL00123.

Pritchett, P. L. (1994), Effect of electron dynamicson collisionless reconnection in two-dimensional magnetotail equilibria, *J. Geophys. Res.*, *99 (A4)*, 5935–594.

Pritchett, P. L., and J. Büchner (1995), Collisionless reconnection in configurations with a minimum in the equatorial magnetic field and with magnetic shear, *J. Geophys. Res.*, *100*, 3601.

Pritchett, P. L., and F. V. Coroniti (2011), Plasma sheet disruption by interchange-generated flow intrusions, *Geophys. Res. Lett.*, *38*, L10,102, doi:10.1029/2011GL047527.

Quest, K., H. Karimabadi, and M. Brittnacher (1996), Consequences of particle conservation along a flux surface for magnetotail tearing, *J. Geophys. Res.*, *101 (A1)*, 179–183, doi:10.1029/95JA02986.

Raeder, J., D. Larson, W. Li, L. Kepko, and T. Fuller-Rowell (2008), OpenGGCM simulations for the THEMIS mission, *Space Sci. Rev.*, *141*, 535–555, doi:10.1007/s11214-008-9421-5.

Raeder, J., P. Zhu, Y. Ge, and G. Siscoe (2010), Open Geospace General Circulation Model simulation of a substorm: Axial tail instability and ballooning mode preceding substorm onset, *J. Geophys. Res.*, *115*, A00I16, doi:10.1029/2010JA015876.

Saito, M. H., L. N. Hau, C. C. Hung, Y. T. Lai, and Y. C. Chou1 (2010), Spatial profile of magnetic field in the near-Earth plasma sheet prior to dipolarization by THEMIS: Feature of minimum B, *Geophys. Res. Lett.*, *37*, L08,106, doi:10.1029/2010GL042813.

Saito, M. H., D. Fairfield, G. Le, L. N. Hau, V. Angelopoulos, J. P. McFadden, U. Auster, J. W. Bonnell, and D. Larson (2011), Structure, force balance, and evolution of incompressible crosstail current sheet thinning, *J. Geophys. Res.*, *116*, A10,217, doi: 10.1029/2011JA016654.

Schindler, K. (1972), A self-consistent theory of the tail of the magnetosphere, in *Earth's Magnetospheric Processes*, edited by B. M. McCormac, p. 200, D. Reidel, Norwell, Mass.

Schindler, K. (1974), A theory of the substorm mechanism, *J. Geophys. Res.*, *79*, 2803–2810.

Sergeev, V. A., T. I. Pulkkinen, R. J. Pellinen, and N. A. Tsyganenko (1994), Hybrid state of the tail magnetic configuration during steady convection events, *J. Geophys. Res.*, *99*, 23,571–23,582, doi:10.1029/94JA01980.

Sitnov, M. I., and M. M. Swisdak (2011), Formation of dipolarization fronts as a part of the magnetic reconnection onset process in two-dimensional current sheets, abstract SM13C-2093 presented at 2011 Fall Meeting, AGU, San Francisco, Calif., 5-9 Dec.

Sitnov, M. I., A. S. Sharma, P. N. Guzdar, and P. H. Yoon (2002), Reconnection onset in the tail of earth's magnetosphere, *J. Geophys. Res.*, *107*, 1256.

Sitnov, M. I., N. Buzulukova, M. Swisdak, V. G. Merkin, and T. E. Moore (2013), Spontaneous formation of dipolarization fronts and reconnection onset in the magnetotail, *Geophys. Res. Lett.*, *40*, 1–6, doi:10.1029/2012GL054701.

Sovinec, C., A. Glasser, D. Barnes, T. Gianakon, R. Nebel, S. Kruger, D. Schnack, S. Plimpton, A. Tarditi, M. Chu, and the NIMROD Team (2004), Nonlinear magnetohydrodynamics with high-order finite elements, *J. Comput.Phys.*, *195*, 355.

Sundaram, A. K., and D. H. Fairfield (1997), Stability of resistive MHD tearing and ballooning modes in the tail current sheet, *J. Geophys. Res.*, *102*, 19,913–19,926, doi:10.1029/97JA01241.

Ugai, M. (1989), Computer studies of a large-scale plasmoid driven by spontaneous fast reconnection, *Phys. Fluids B*, *1*(4), 942–948, doi:10.1063/1.859018.

Zhu, P., and J. Raeder (2013), Plasmoid formation in current sheet with finite normal magnetic component, *Phys. Rev. Lett.*, *110*, 235,005, doi:10.1103/PhysRevLett.110.235005.

Zhu, P., J. Raeder, K. Germaschewski, and C. C. Hegna (2009), Initiation of ballooning instability in the near-Earth plasma sheet prior to the 23 March 2007 THEMIS substorm expansion onset, *Ann. Geophys.*, *27*, 1129–1138.

Zhu, P., J. Raeder, C. C. Hegna, and C. R. Sovinec (2013), Nature of axial tail instability and bubble-blob formation in near-earth plasma sheet, *J. Geophys. Res. Space Physics*, *118*, 653–663, doi:10.1029/2012JA017972.

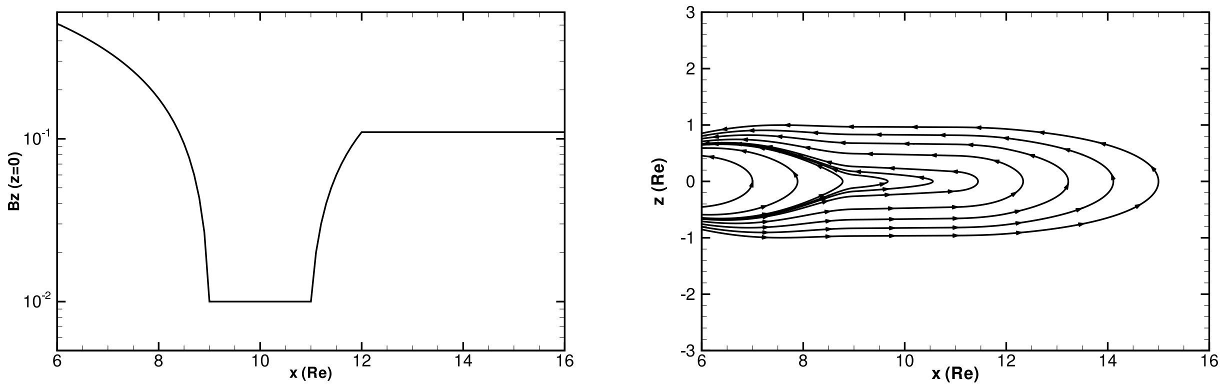

Figure 1. The piece-wise continuous $B_{0z}(x,0)$ profile defined in Eq. 1 (left) and the corresponding magnetic field streamlines (right) of the near-Earth magnetotail model.

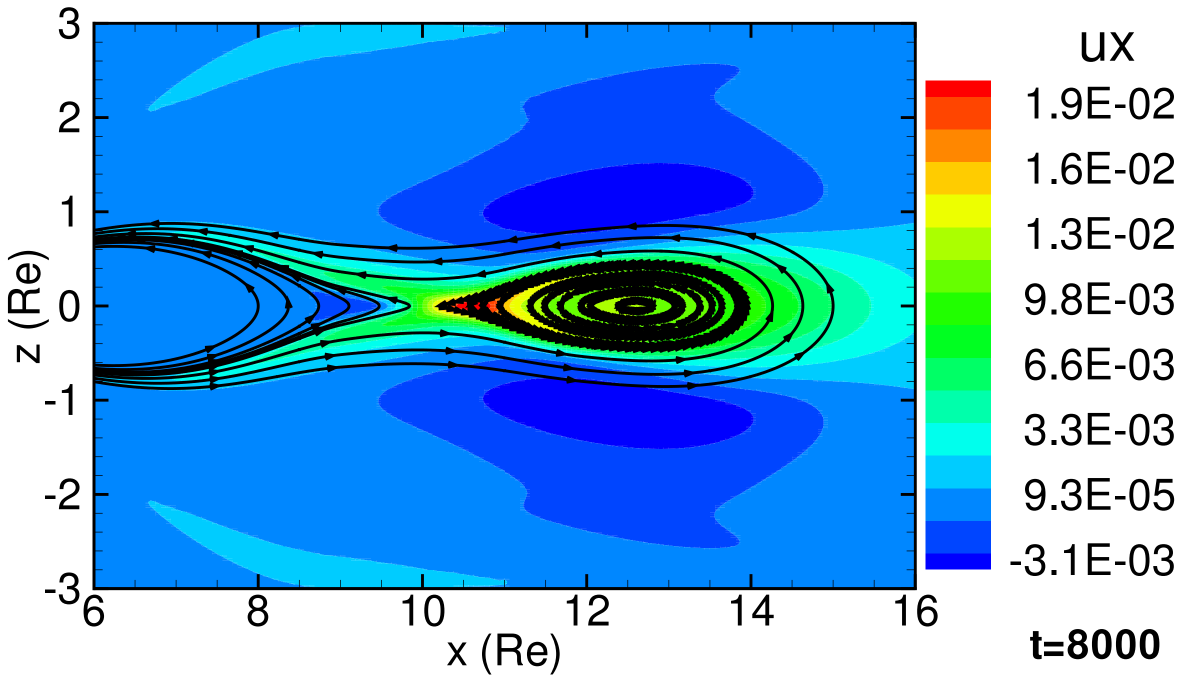

Figure 2. Contour of tailward component of velocity field and streamlines from 2D projection of magnetic field in the $x-z$ plane at $t = 8000$ following the nonlinear development of the 2D resistive tearing or axial tail mode.

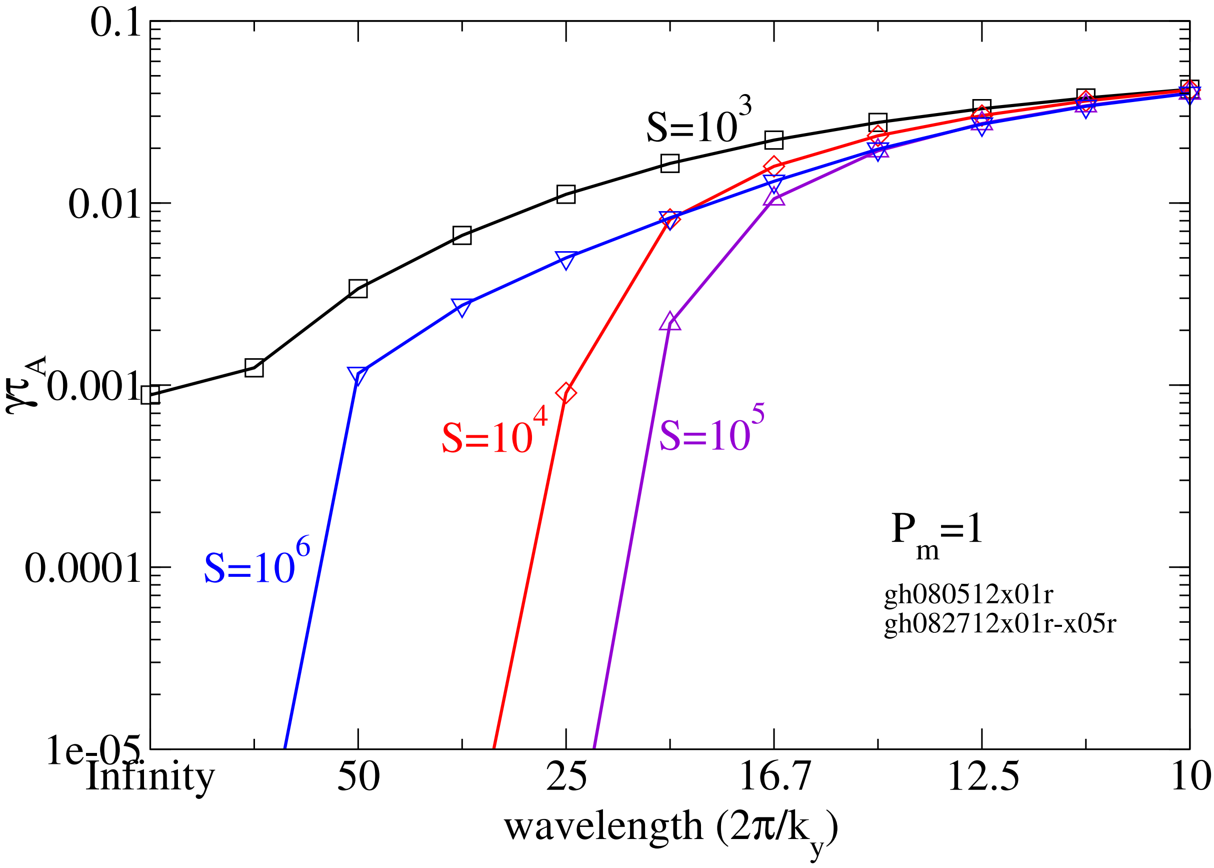

Figure 3. Linear growth rates as function of the wavelength in y direction for different regimes of Lundquist number S. The magnetic Prandtl number $P_m \equiv \mu/\eta = 1$ for all cases.

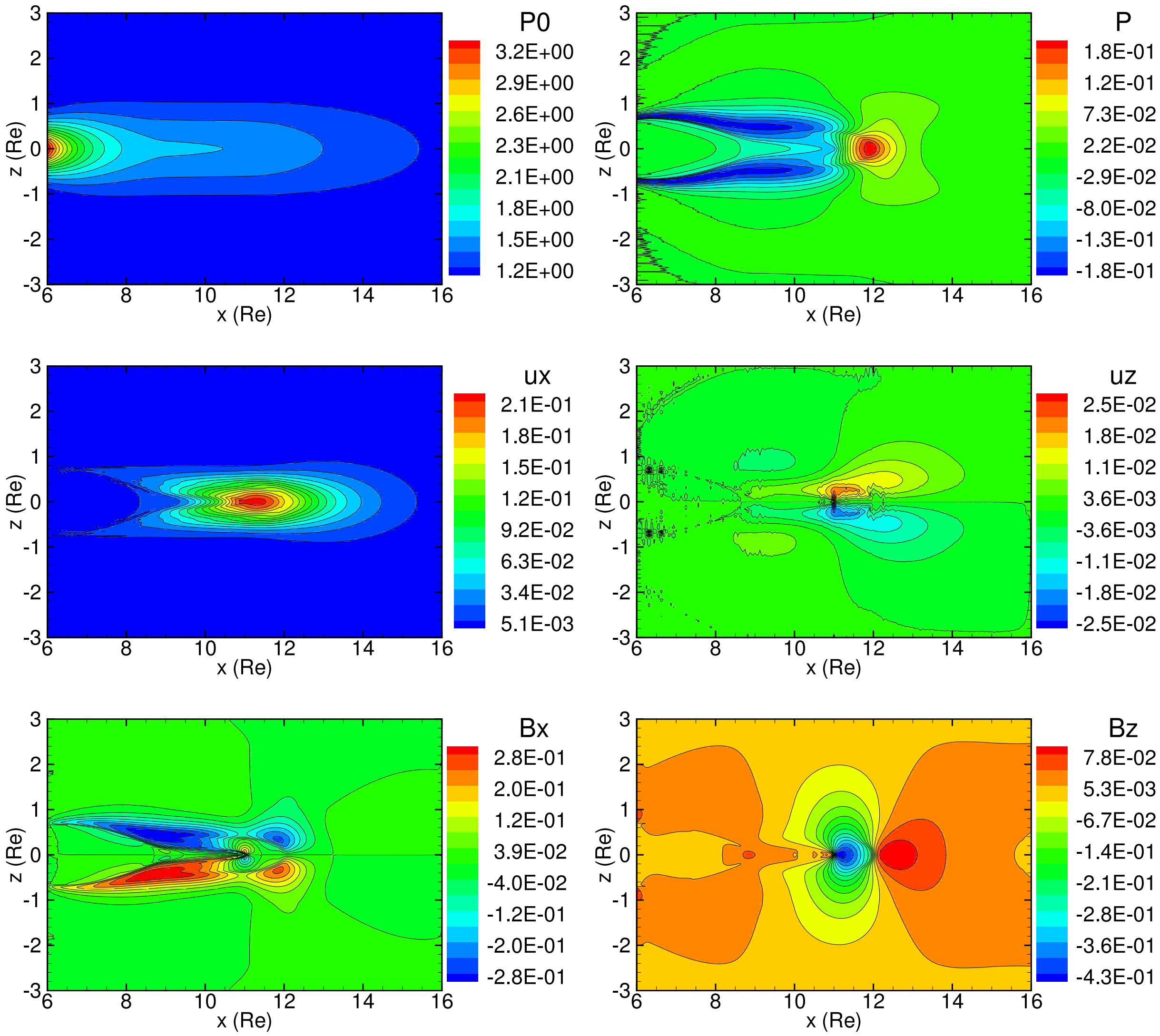

Figure 4. Contours of equilibrium pressure (top left), and perturbed pressure (top right), x component of perturbed flow (middle left), z component of perturbed flow (middle right), x component of perturbed magnetic field (bottom left), and z component of perturbed magnetic field (bottom right) in the $x-z$ plane for a linear $k_y = 0.2\pi$ ballooning instability.

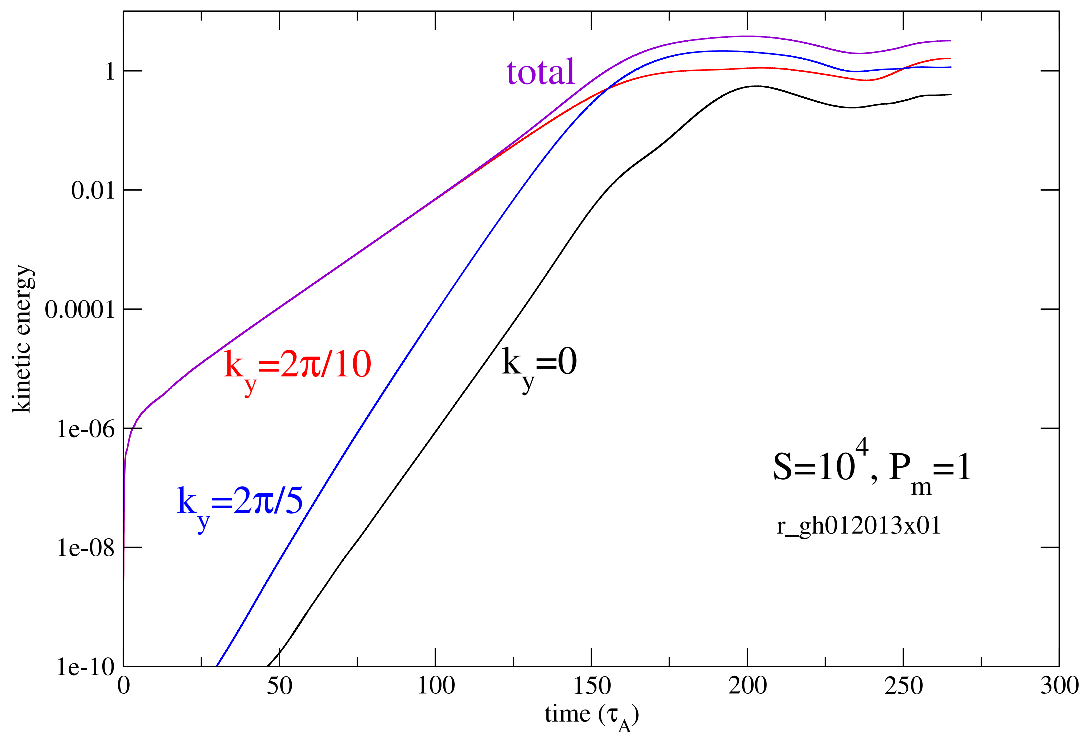

Figure 5. Growth of the kinetic energies of $k_y = 0$ (black line), $k_y = 0.2\pi$ (red line), and $k_y = 0.4\pi$ components, and the total energy (purple line) of the nonlinear perturbation.

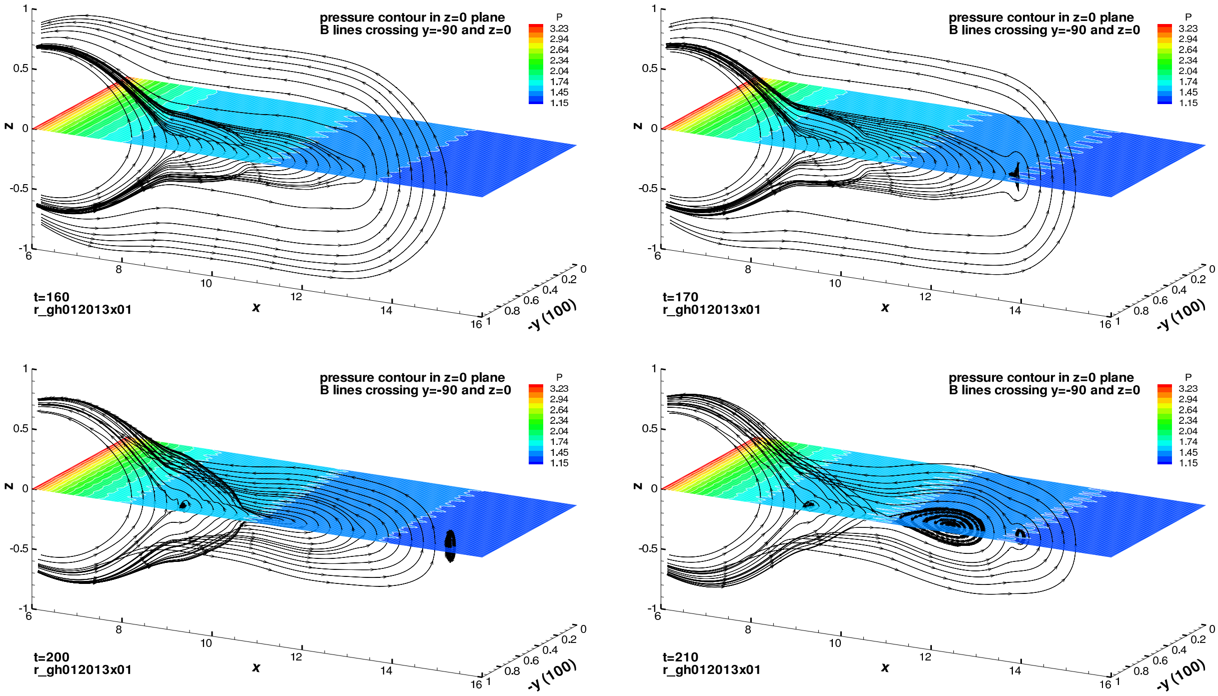

Figure 6. Total pressure contours in the $z = 0$ plane and magnetic field streamlines crossing the x axis at $y = -90, z = 0$ at selected times ($t = 160, 170, 200, 210$) of the nonlinear development.

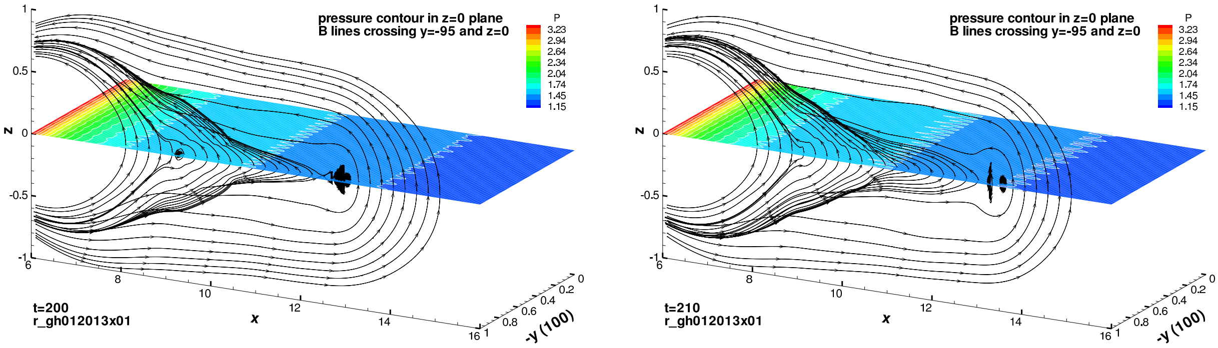

Figure 7. Total pressure contours in the $z = 0$ plane and magnetic field streamlines crossing the x axis at $y = -95, z = 0$ at selected times ($t = 200, 210$) of the nonlinear development.

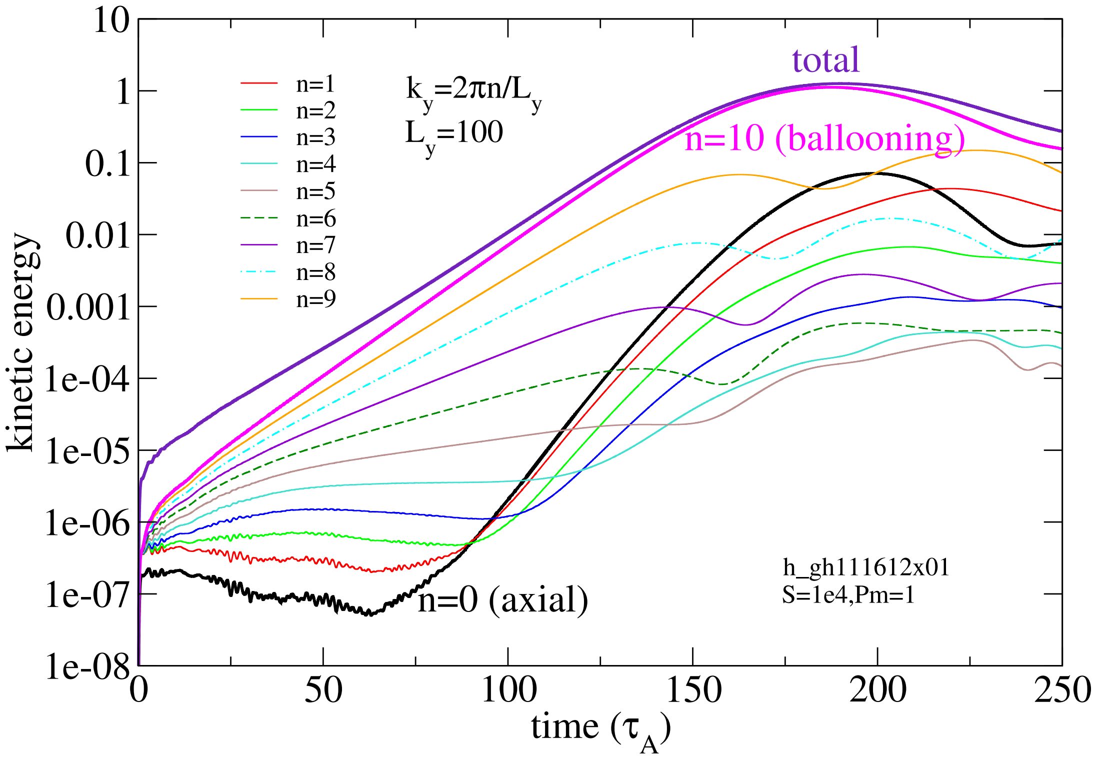

Figure 8. Kinetic energies of all Fourier components in the y direction of the perturbation as function of time.

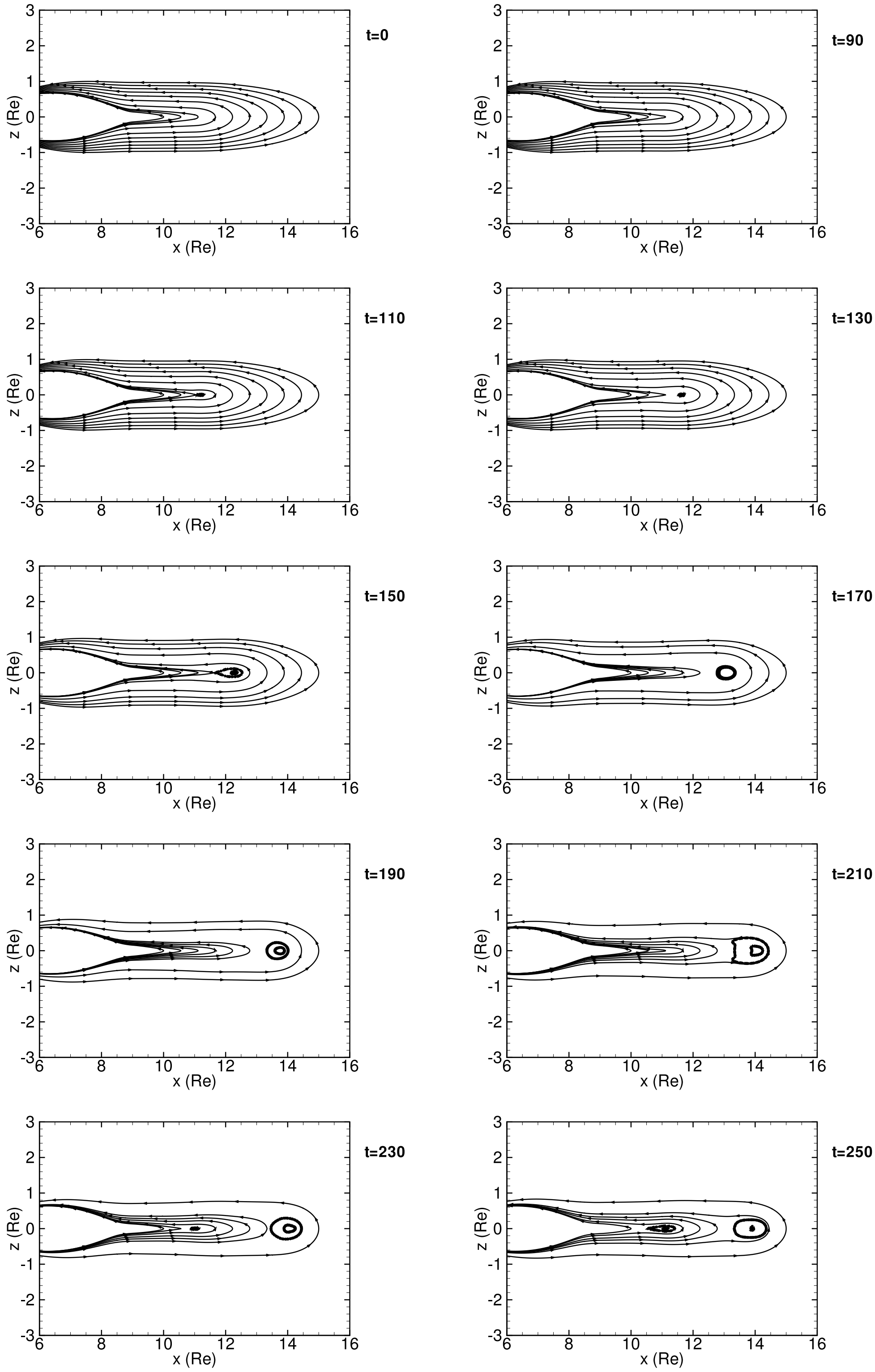

Figure 9. Time evolution of the 2D projection of magnetic field streamlines in the $x-z$ ($y = 0$ or $y = -100$) plane.

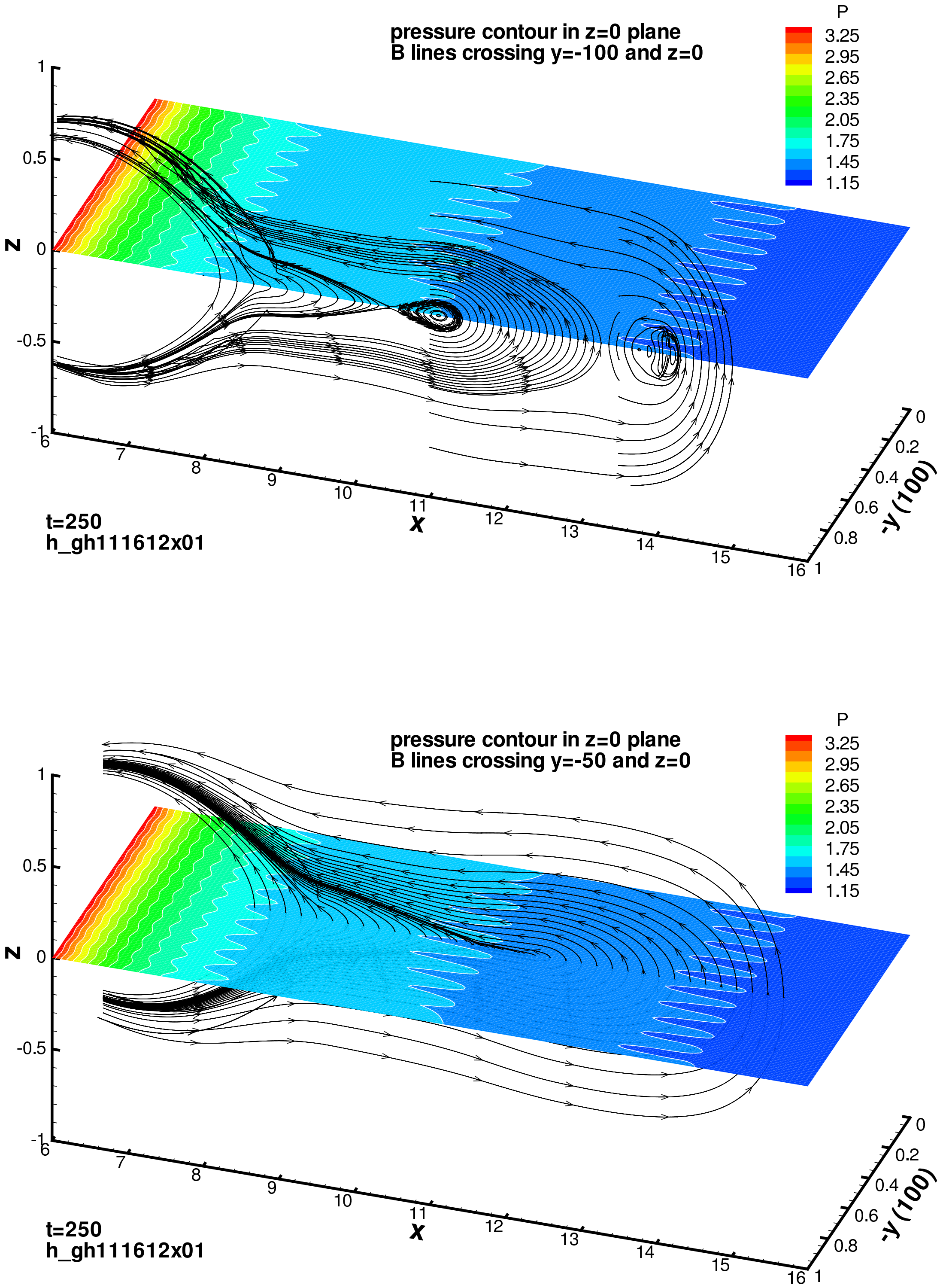

Figure 10. Contours of total pressure in the $z = 0$ plane and magnetic field streamlines crossing the x axes at $z = 0$ and $y = -100$ (top panel), and $z = 0$ and $y = -50$ (bottom panel) at the time $t = 250$.

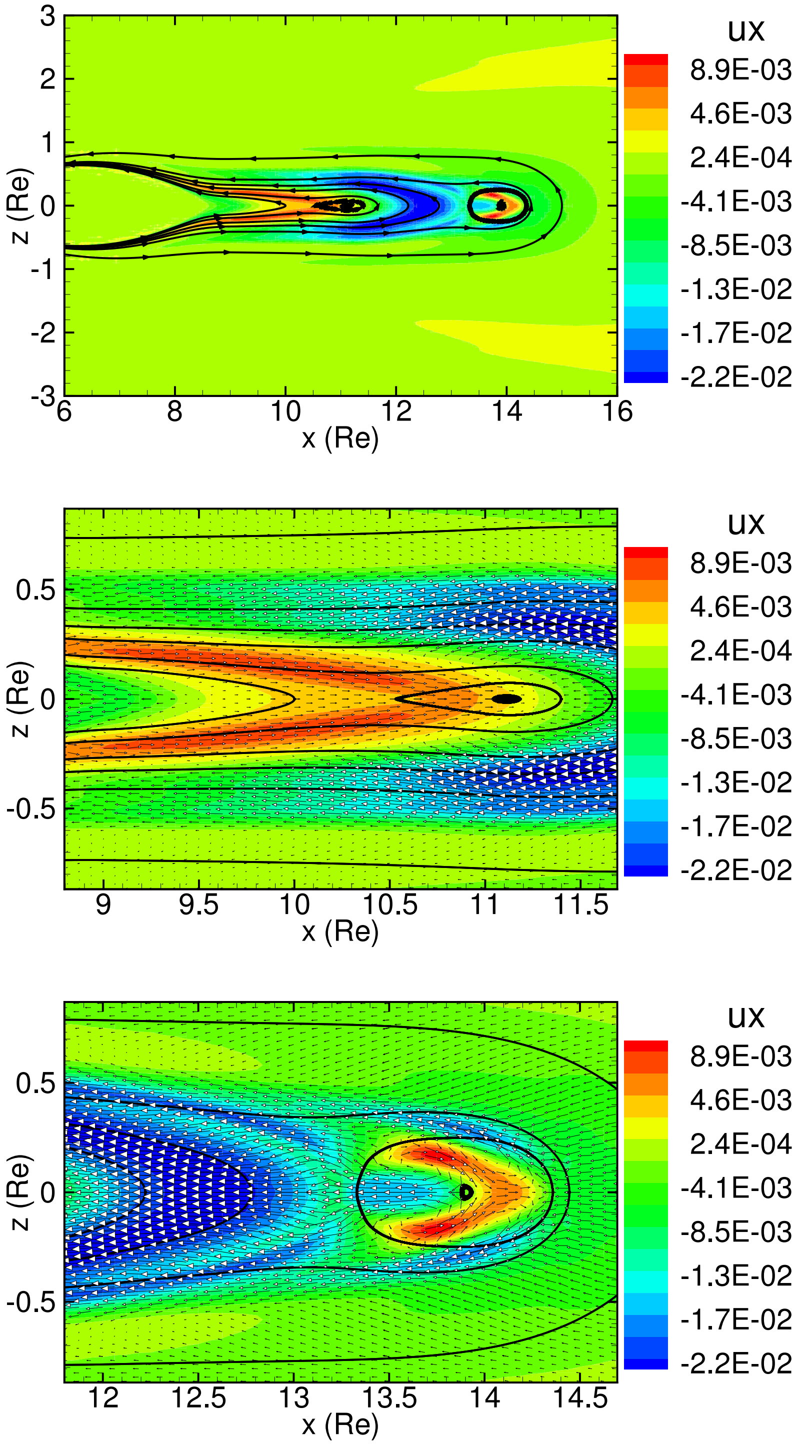

Figure 11. Top panel: Contours of x component of flow field and 2D projection of magnetic field streamlines in $x - z$ ($y = 0$ or $y = -100$) plane; Middle panel: Zoomed-in view of the plasmoid structure closer to the Earth; Bottom panel: Zoomed-in view of the plasmoid structure farther away from the Earth. The arrows in middle and bottom panels represent 2D projection of the flow vector field in $x - z$ ($y = 0$ or $y = -100$) plane.

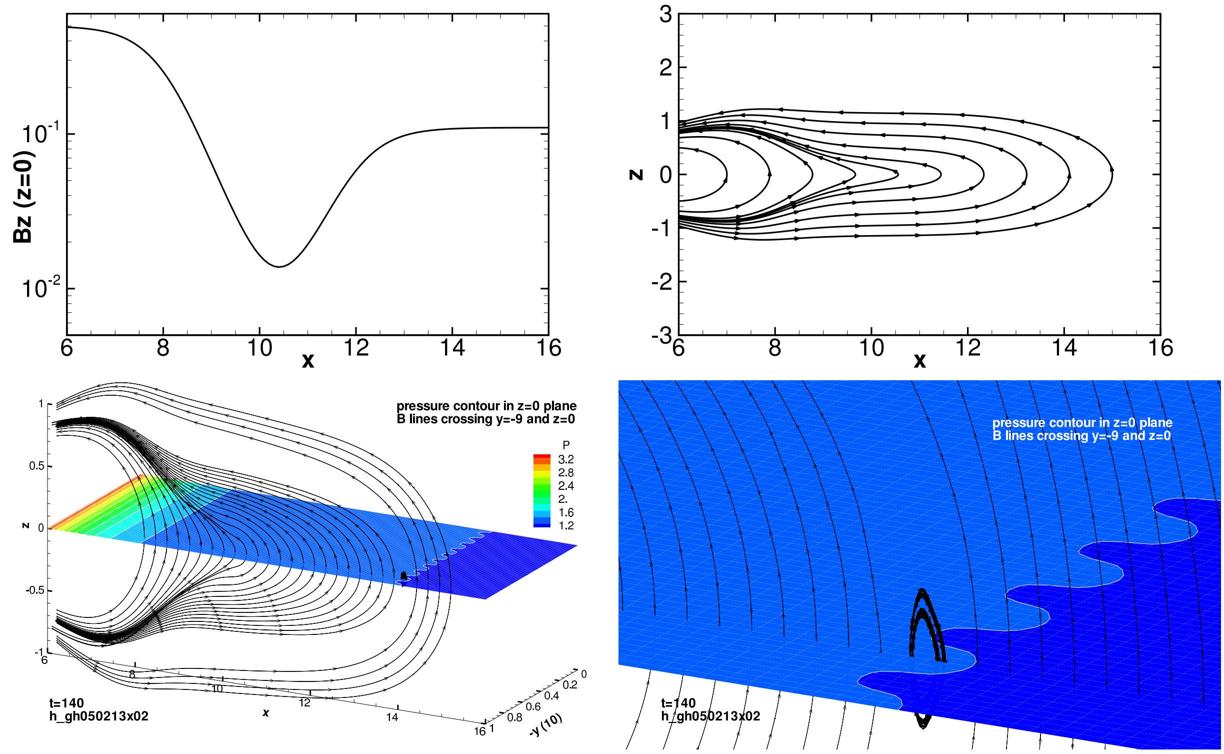

Figure 12. Upper row: Smooth $B_{0z}(x, 0)$ profile defined by Eq. (8) (left) and the corresponding magnetic field streamlines (right) of the near-Earth magnetotail model; Lower row: pressure contour in $z = 0$ plane and magnetic field streamlines crossing $y = -9$ and $z = 0$ at $t = 140$ (left); Zoomed-in view of the plasmoid structure in the lower left panel near $x = 14$, $y = -9$, and $z = 0$ (right).